

## Synthesis, characterization and biophysical evaluation of the 2D Ti<sub>2</sub>CT<sub>x</sub> MXene using 3D spheroid-type cultures



Gim Pao Lim <sup>a</sup>, Chin Phong Soon <sup>a,\*</sup>, Agnieszka Maria Jastrzębska <sup>d</sup>, Nyuk Ling Ma <sup>c</sup>, Anita Rozmysłowska Wojciechowska <sup>d</sup>, Aleksandra Szuplewska <sup>d</sup>, Wan Ibtisam Wan Omar <sup>a</sup>, Marlia Morsin <sup>a</sup>, Nafarizal Nayan <sup>a</sup>, Kian Sek Tee <sup>b</sup>

<sup>a</sup> Biosensor and Bioengineering Lab, Microelectronics and Nanotechnology-Shamsuddin Research Center, Institute for Integrated Engineering, Universiti Tun Hussein Onn Malaysia, 86400, Parit Raja, Batu Pahat, Johor, Malaysia

<sup>b</sup> Faculty of Electrical and Electronic Engineering, Universiti Tun Hussein Onn Malaysia, 86400, Parit Raja, Batu Pahat, Johor, Malaysia

<sup>c</sup> Faculty of Science and Marine Environment, Universiti Malaysia Terengganu, 21030, Kuala Nerus, Terengganu, Malaysia

<sup>d</sup> Faculty of Materials Science and Engineering, Warsaw University of Technology, 02-507, Warsaw, Wolska 141, Poland

### ARTICLE INFO

#### Keywords:

MAX phase  
MXenes  
Ti<sub>2</sub>CT<sub>x</sub>  
Cytotoxicity *in vitro*  
3D cell model  
Spheroids

### ABSTRACT

MXenes are novel 2-D materials which have been extensively investigated for use in advanced biocomposites, water purification, biosensors, bioimaging and antibacterial systems. However, the knowledge associated with the mechanism of cytotoxic response is still limited to lack of verification against 3D spheroid-type cultures. Herein, we present a report on the *in vitro* cytotoxicity of Ti<sub>2</sub>CT<sub>x</sub> MXene against cervical cancer cell lines (HeLa) in a form of 3D spheroid with comparison to 2D cell culture system. Ti<sub>2</sub>CT<sub>x</sub> MXenes can be characterized by their multi-layered structure that is produced by the efficient elimination of Al and appearance of the surface functional groups. The biological results with 2D and 3D HeLa indicated that the Ti<sub>2</sub>CT<sub>x</sub> MXene was moderately cytotoxic to cells and the cytotoxicity was dose dependent. Our results showed that the toxicity of MXenes is potentially due to direct contact of the Ti<sub>2</sub>CT<sub>x</sub> MXene with the cell membrane wall. The Raman spectra suggested that the Ti<sub>2</sub>CT<sub>x</sub> MXenes interfered with the cytoplasmic proteins' conformation and the surrounding microenvironment. This inherently modified the biochemistry of the cell membrane and caused cell apoptosis. This paper contributes to the pool of knowledge regarding the biocompatibility and biophysical properties of Ti<sub>2</sub>CT<sub>x</sub> MXene.

### 1. Introduction

MXenes are a group of novel 2-D materials that was first developed by researchers in Drexel University in 2011 [1]. They typically consist of early transition metal carbides, and nitrides. Among them, Ti<sub>3</sub>C<sub>2</sub>T<sub>x</sub> is the most studied MXene. The 'T<sub>x</sub>' in Ti<sub>3</sub>C<sub>2</sub>T<sub>x</sub> represents the surface terminating functional groups such as –O, –OH, and –F. The unique properties of MXenes such as their electronic conductivity, hydrophilicity, high surface-area-to-volume-ratio, excellent near-infrared absorption, and antimicrobial properties have received wide attention in fields relating to biological and biomedical applications. Indeed MXenes have many applications in the field of biocomposites, bioimaging, biosensors, cancer theranostics, energy storage, electromagnetic interference shielding, water purification, as well as photochemical catalysis [2].

Our first studies on the *in vitro* cytotoxicity of delaminated MXenes [3] showed that Ti<sub>3</sub>C<sub>2</sub>T<sub>x</sub> MXene exhibits toxicity against cancer cells

while only slightly impacting non-malignant cells. The proposed mechanism against cancer cells and non-malignant ones is due to stress caused by reactive oxygen species (ROS) that is generated *in situ* [3]. Scheibe et al. [4] studied the cytotoxic effects of Ti<sub>3</sub>C<sub>2</sub>T<sub>x</sub> MXenes and their precursors on human fibroblasts and HeLa cells *in vitro*. The results showed that exposure to a high concentration of Ti<sub>3</sub>C<sub>2</sub>T<sub>x</sub> and MAX phase up to 400 µg/mL induced significant cytotoxicity effects via oxidative and mechanical stress generation. Authors additionally suggested that Ti<sub>3</sub>C<sub>2</sub>T<sub>x</sub> MXene was cyto-compatible with cell viability at more than 80% for concentrations between 10 and 400 µg/mL [4]. They also revealed that the cytotoxic behavior of Ti<sub>3</sub>C<sub>2</sub>T<sub>x</sub> was dependent on cell type, with higher cytotoxicity observed for HeLa cells compared to human fibroblasts cells. We were the first to synthesize Ti<sub>2</sub>C MXene surface-modified with polyethylene glycol (PEG) as a novel selective agent for photothermal therapy [5]. The Ti<sub>2</sub>C/PEG showed good biocompatibility with cell viability achieving more than 70% at all tested

\* Corresponding author.

E-mail address: [soon@uthm.edu.my](mailto:soon@uthm.edu.my) (C.F. Soon).

concentrations (62.5–500 µg/mL) [5]. Above this concentration range, ROS generation may be responsible for the cytotoxicity of the Ti<sub>2</sub>C MXene. The cytotoxicity of single-layered MXenes that includes Ti<sub>2</sub>CT<sub>x</sub> and Ti<sub>3</sub>C<sub>2</sub>T<sub>x</sub> have been examined *in vitro* using only the two-dimensional (2D) cell culture system. To the best of our knowledge, *in vitro* cytotoxicity evaluation of MXenes using three-dimensional (3D) cell culture system (also called spheroid) has not been explored yet.

Therefore, we present an original study on the cytotoxicity of Ti<sub>2</sub>CT<sub>x</sub> MXene in a colloidal suspension using a 3D spheroid system. We performed material synthesis, characterization as well as evaluation of its cytotoxic properties.

## 2. Materials and methods

Ti<sub>2</sub>AlC MAX phase powder was commercially purchased from Advanced 2D Materials CO. Ltd., Beijing, China. Ethanol (98%) and hydrofluoric acid (HF, 49% in H<sub>2</sub>O) of analytical grade were purchased from Merck, Germany. Dulbecco's Modified Eagle Medium (DMEM), Hank's Balanced Salt Solution (HBSS), streptomycin (100 mg/mL), fungizone (2.5 mg/L), 10% fetal calf serum, trypsin (0.25%), penicillin (100 units/mL), dimethyl sulfoxide (DMSO) (0.01 M), and formaldehyde (2.5 %v/v), were purchased from Sigma Aldrich, Dorset, UK. For assay tests, MTT assay was purchased from Sigma Aldrich, UK. Live/dead cell viability kit was purchased from Life Technologies, California, US and Muse<sup>TM</sup> Count & Viability kit was purchased from Luminex, US.

### 2.1. Preparation of Ti<sub>2</sub>CT<sub>x</sub> MXene

1 g of Ti<sub>2</sub>AlC MAX phase was slowly added to 20 mL of HF and then the solution was stirred for 24 h at 25 °C. Then, HF is used to etch away the aluminum (Al) and then the Ti<sub>2</sub>CT<sub>x</sub> sediments is washed with deionized water and centrifuged for 5 min at 3500 rpm. This washing step was repeated until the supernatant reaches pH 6. The sediment which is etched Ti<sub>2</sub>CT<sub>x</sub> multilayers was dried at 80 °C for 12 h in an oven. Subsequently, 0.8 g of the multilayers Ti<sub>2</sub>CT<sub>x</sub> powder was added to 20 mL of ethanol and stirred for 24 h. Then, the ex-Ti<sub>2</sub>CT<sub>x</sub> solution was ultra-sonicated for 2 h and then subject to centrifugation for 5 min at 3500 rpm. Finally, the supernatant was collected and dried at 80 °C for 12 h in an oven.

### 2.2. Characterization of the MXene

#### 2.2.1. Field-emission scanning electron microscopy

The micrographs showing the surface and edge-view morphology of the Ti<sub>2</sub>AlC MAX phase and Ti<sub>2</sub>CT<sub>x</sub> MXene were obtained using a field-emission scanning electron microscope model JSM-7600F (FE-SEM, JOEL, Tokyo, Japan) equipped with an upper secondary electron imaging (SEI) detector. Elements present on the surface were inspected using an energy dispersive X-ray (EDX, 10 keV) with an EMAX energy spectrometer (HORIBA, Ltd., Kyoto, Japan). The elemental composition of Ti<sub>2</sub>CT<sub>x</sub> was also inspected.

#### 2.2.2. High-resolution transmission electron microscope

The 2D multilayered structure of Ti<sub>2</sub>C particles in 10 mg was placed on Cu-C mesh and examined in an edge-on orientation and analyzed by using a high-resolution transmission electron microscope (HREM, Philips CM 20). Fourier transformation (FFT) and reversed fourier transformation (IFFT) analysis were used for atomic-scale investigations of layers stacking and thickness. The selected area diffraction pattern (SADP) of the electrons showed characteristic layered lattice from which we measured the interplanar distance.

#### 2.2.3. X-ray diffraction spectroscopy (XRD)

X-ray diffraction spectroscopy (XRD) (PANalytical, Netherlands) with a Cu  $\kappa\alpha$  X-ray source ( $\lambda = 1.54 \text{ \AA}$ ) was used to analyze the elemental composition of the Ti<sub>2</sub>AlC and Ti<sub>2</sub>CT<sub>x</sub> MXene using a step size of 0.03°

and a scan speed of  $0.06 \text{ }^{\circ}\text{s}^{-1}$ . Measurement was carried out in a 20 range of 5–80°. A thin layer of MAX phase or MXene was deposited on a glass substrate, and the prepared substrate was put on a glass slide for the XRD analysis.

#### 2.2.4. Raman spectroscopy

Raman spectra of the Ti<sub>2</sub>AlC MAX phase and Ti<sub>2</sub>CT<sub>x</sub> MXene were obtained using a Raman spectroscope (Horiba Xplus, USA) equipped with a 532 nm laser source. For sample preparation, the particles of MAX phase or MXene were deposited on a glass slide and examined with a laser power. This analysis was conducted to inspect the presence of terminating functional groups on the surface of MAX phase and delaminated MXene.

#### 2.2.5. Zeta potential and dynamic light scattering measurement

The MXene was treated with CaCl<sub>2</sub> and sodium alginate to analyze its stability in aqueous solutions, which was determined using the zeta potential measurements. This verified that MXene/alginate could allow MXene and 3D cells interactions. NANO ZS ZEN3500 analyzer (Malvern Instruments, Malvern, UK) with a back-scattered light detector using a 173° dispersive angle is used to carry out zeta potential and dynamic light scattering (DLS) analysis. The 2D Ti<sub>2</sub>C MXene particles were tested at a concentration of  $5 \times 10^{-5} \text{ g mL}^{-1}$  at different concentrations of sodium alginate. This approach generated a differing weight ratio of sodium alginate to MXene ranging from 1:0 to 1:20 and was already validated in previous studies [6–8]. The zeta potential of 2D Ti<sub>2</sub>CT<sub>x</sub> modified with CaCl<sub>2</sub> was measured at a weight ratio of 1:1. Each sample was mildly homogenized for 30 s and the zeta potential and DLS study were performed at room temperature (25 °C). The DLS and zeta potential are expressed as the mean value of sheet diameter and zeta potential ± standard deviation (SD), respectively.

#### 2.2.6. FTIR measurements

FTIR measurements were carried out using a Thermo Scientific FT-IR Nicolet iS5 Spectrometer within a diffuse reflectance infrared Fourier transform spectroscopy (DRIFTS) technique with operating wavelengths ranging from 220 to 4000 cm<sup>-1</sup>. To perform the measurements, pristine Ti<sub>2</sub>CT<sub>x</sub> MXene particles unmodified and modified with sodium alginate and CaCl<sub>2</sub> were incorporated into dry KBr to a concentration of 2.5 wt%. Each of the spectrum was reported as an average of 30 scans. A Thermo Fisher analysis software (OMNIC<sup>TM</sup> Spectra) was used for data analysis.

#### 2.2.7. UV-Vis measurement

The homogenized aqueous solutions of 2D Ti<sub>2</sub>CT<sub>x</sub> MXene particles were modified with sodium alginate (1 wt%) in a ratio of 1:1 as well as 2D Ti<sub>2</sub>CT<sub>x</sub> MXene, sodium alginate, and CaCl<sub>2</sub> in a ratio 1:1:0.5 at a concentration of  $5 \cdot 10^{-5} \text{ g mL}^{-1}$ . Such prepared colloidal solutions were tested using UV-Vis spectrometer (Evolution 220, Thermo Scientific). Each spectrum was recorded in the 220–1100 nm range, 200 nm min<sup>-1</sup> scan speed, 0.30 s of integration time, and 1.00 nm resolution.

### 2.3. Biophysical analysis

#### 2.3.1. Cell culture

HeLa cell lines were cultured in a Dulbecco modified eagle medium that consist of 10% fetal calf serum, 2.5 mg/L of fungizone, 100 mg/mL of streptomycin, and also 100 units/mL of penicillin. The culture is incubated at 37 °C with 5% CO<sub>2</sub>. When the confluence reaches 80%, the media was discarded, and the cells were washed thrice using Hank's Balance Salt Solution (HBSS). Then, 1 mL of 0.5 mg/L trypsin was added to the flask before it was further incubated for another 5 min at 37 °C under a 5% CO<sub>2</sub> atmosphere. Then 5 mL of DMEM was used to quench the trypsinization. The HeLa cells was retrieved by centrifuging at 1000 rpm for 5 min.

### 2.3.2. Cytotoxicity assay

HeLa cells were used to study the cellular toxicity effects of MXenes *in vitro*. Cells ( $1 \times 10^4$  cells/mL) were put in to 96-well plates and allowed to incubate overnight at 37 °C under a 5% CO<sub>2</sub> atmosphere. Then, the old medium was discarded and replaced with a new medium containing MXenes at different concentrations (50 to 500 µg/mL). The samples were further incubated for 24 h. The control contained only cells and culture media in the 96 well plate. The cytotoxicity of the MXenes on HeLa cells was determined by MTT assay. After incubation, cells were washed with HBSS and exposed to a MTT solution (10 mg/mL in HBBS; 100 µL per well). Then, the cells were incubated in MTT assay for 4 h and kept in the dark. Then, the supernatant was discarded and violet formazan crystals was found to have formed. The crystals were redissolved in dimethyl sulfoxide (DMSO, 100 µL per well) and its absorbance is measured at  $\lambda = 570$  nm. The results are expressed as the percentage viability over the control groups. The experiments were performed in triplicate.

### 2.3.3. Cell viability assay using live/dead cell staining

The culture adherent cells previously co-incubated for 24 h with 50 or 500 µg/mL of MXene were prepared on glass slides. Cells not exposed to MXene were used as the positive control. The cells were washed with a phosphate buffered saline solution (PBS, pH 7.4) before use. To observe the cell viability by using the staining kit. Ethidium homodimer (EthD-1) and calcein-AM fluorescent dyes were used to stain the cells. The cells were incubated in the staining reagents for 20 min in the dark. Subsequently, the staining reagents was discarded, and the cells were washed thrice with HBSS. The stained cells can then be imaged using a BX53 fluorescence microscope (Olympus, Tokyo, Japan), mounted with a DP-2 monochrome charged-coupled device (CCD) camera. The experiments are carried out in triplicate.

### 2.3.4. Flow cell

Cell viability was also determined using Muse™ Count & Viability reagent. Cells ( $1 \times 10^5$  cells/mL) were incubated overnight at 37 °C under a 5% CO<sub>2</sub> atmosphere. Then, the old medium was discarded and replaced with a new medium containing MXenes (50 to 500 µg/mL) at differing concentrations. The sample was further incubated for another 24 h. After cell incubation, the cells were washed thrice with HBSS. 0.2 mL of trypsin (0.5 mg/L) was added, and the sample was incubated for 5 min at 37 °C with 5% CO<sub>2</sub>. Then, 0.2 mL of DMEM was used to stop the trypsinization process. The sample were centrifuged at 1000 rpm for 5 min. Then, 20 µL of cell suspensions were added to 380 µL of the count & viability reagent in each tube and incubated for 5 min at room temperature. The percentage of cell viability (%) was then analyzed using the Muse® Cell Analyzer.

### 2.3.5. Oxidative stress of cells

The oxidative stress level was determined using a Muse® oxidative stress kit. HeLa cells were incubated with 50 and 500 µg/mL of Ti<sub>2</sub>CT<sub>x</sub> MXenes for 24 h. Subsequently, cells were loaded with an assay buffer (Muse® Oxidative Stress Kit) for 30 min at 37 °C. The oxidative stress level of cells was then measured using the Muse® Cell Analyzer.

### 2.3.6. Evaluation of cytotoxicity of MXenes in 3D cell culture

Spheroids of HeLa cells were synthesized through a flicker micro-encapsulation technique. About 100 µL of cell pellets with density  $1.5 \times 10^8$  cells/mL were stirred into a 2% w/v sodium alginate solution and put into an insulin syringe. After flicking for 5 min, the microbeads which encapsulate the HeLa cells were soaked in the chloride solution for 20 min. The microbeads were then retrieved and cultured in 3 mL DMEM. The microbeads containing cell spheroids were allowed to grow for 15 days. The microbeads after 15 days were washed with HBSS and treated with 50 and 500 µg/mL of Ti<sub>2</sub>CT<sub>x</sub> MXenes for 24 h. After treatment, the microbeads containing spheroid cells were then stained using 2 µm of calcein-AM and 4 µm of EthD-1 solution and kept in the

dark for 20 min. Then, the fluorescent dye solution was discarded and the microbead encapsulated cells were washed thrice with HBSS. The cells in the microbeads were inspected using a BX53 fluorescence microscope (Olympus, Tokyo, Japan). The alginate shell of the alginate microbeads of HeLa cells was removed by using alginate lyase and the 3D microtissues released from the alginate membrane were treated with 500 µg/mL of the Ti<sub>2</sub>CT<sub>x</sub> MXenes. The live/dead cell viability kit was used to stain cells in the microtissues as described in section 2.3.3.

### 2.3.7. Phase contrast microscopy

HeLa cells were cultured under 5% CO<sub>2</sub> atmosphere at 37 °C. Then, 50 or 500 µg/mL Ti<sub>2</sub>CT<sub>x</sub> MXene in DMEM solution was introduced to the HeLa cells. After 24 h incubation, HBSS solution was used to wash the cells two times. Then, a series of phase contrast microscopy images were obtained using an inverted phase contrast microscope (TS100, Nikon, and Tokyo, Japan) equipped with a Go-5 CCD digital camera (QImaging, Surrey, UK) to study the morphological changes in cells.

### 2.3.8. Field emission scanning electron microscopy of HeLa cells

The monolayer of HeLa cells are exposed to 50 or 500 µg/mL of MXenes that is dispersed on a glass slide, supplemented with culture medium for 24 h. At the same time, control cells were also dispersed on a glass slide but exposed only to the culture medium for 24 h. Then, cells were washed with HBSS solution and 2.5% formaldehyde was added and the mixture allowed to incubate at 4 °C for 2 h. Then, the cells were re-washed in HBSS and further dehydrated using 70% ethanol. The sample was dried for 12 h and transferred to a FE-SEM sample holder and attached using a conductive adhesive. The sample was then sputter-coated with gold nanoparticles (JFC 1600-Auto fine coated, JOEL, Japan). The scanning electron microscopy was performed using a FE-SEM (JSM-7600F, Jeol, Japan), operating at 5.0 kV.

### 2.3.9. Raman spectroscopy of HeLa cells

HeLa cells were exposed with and without (control) 500 µg/mL of Ti<sub>2</sub>CT<sub>x</sub> MXenes dispersed on glass slides and incubated for 24 h. After treatment, the cells were washed in HBSS solution. Then, the sample was dried for 12 h and placed on a microscope slide for Raman spectroscopy (Horiba Xplora) analysis using a 532 nm laser source.

## 2.4. Statistical analysis

All results are expressed as the mean  $\pm$  standard error of the mean. These are analyzed using a two-tailed Student's t-test. The *p* value less than 0.05 is taken to be significant.

## 3. Results and discussion

### 3.1. Morphological of Ti<sub>2</sub>AlC MAX phase and Ti<sub>2</sub>CT<sub>x</sub> MXene

The FE-SEM image shows that the Ti<sub>2</sub>AlC MAX phase was defined by structures consisting of compact and aluminum-carbide basal plane layers (Fig. 1A(i)). After etching with HF, the Ti<sub>2</sub>AlC which initially had a dense structure was dissociated into loose lamellar layers due to the etching of aluminum (Al) layers. The subsequent dispersion and ultra-sonication processes in ethanol causes further separation of the metal-carbide layers (Fig. 1A(ii)). EDX elemental analysis was performed to inspect the mass ratio of the Ti<sub>2</sub>CT<sub>x</sub> MXene (Fig. 1B). For the MAX phase of Ti<sub>2</sub>AlC, the atomic percentage of the Al in Ti<sub>2</sub>AlC was 5.2% (Fig. 1C). After etching with HF acid and ultra-sonication process in ethanol, the atomic percentage of Al in Ti<sub>2</sub>CT<sub>x</sub> MXene (Fig. 1C) was further reduced to 0.29%. The residual Al after etching is likely due to the formation of AlF<sub>3</sub>, which is difficult to remove completely. The Ti<sub>2</sub>CT<sub>x</sub> MXene is composed of Ti (8.32%), C (59.72%), O (24.39%), F (7.27%) and a trace amount of Al (0.29%) was estimated from EDX analysis (Fig. 1C). This indicates the formation of Ti<sub>2</sub>CT<sub>x</sub> MXene sheets with layers containing -O and -F groups. Similar results have been reported in a previous study

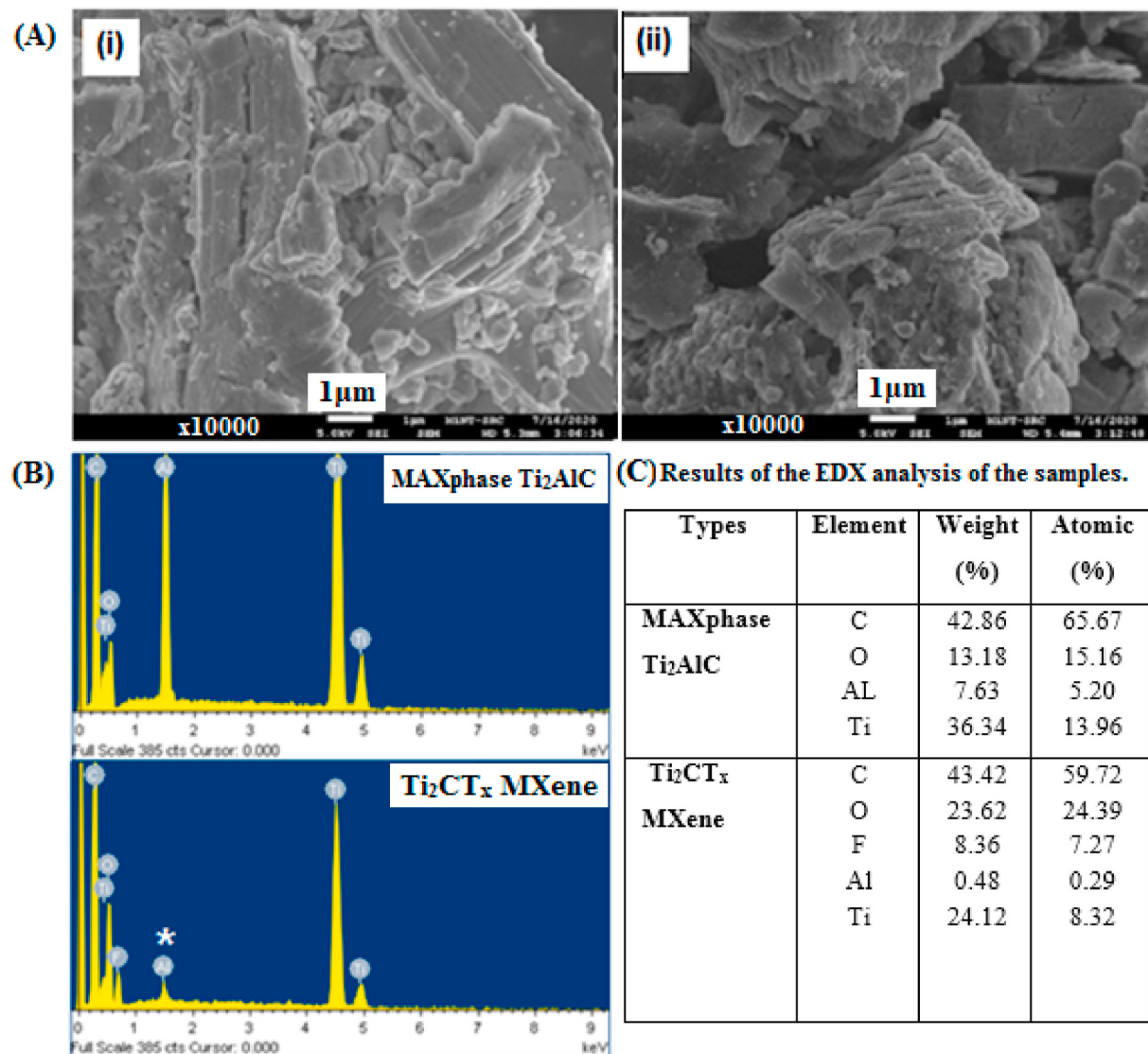


**Fig. 1.** (A) FE-SEM images of (i) Ti<sub>2</sub>AlC MAX phase and (ii) Ti<sub>2</sub>CT<sub>x</sub> MXenes, (B) EDX spectra of weight percentage of MAX phase Ti<sub>2</sub>AlC and Ti<sub>2</sub>CT<sub>x</sub> MXene, (C) Table for elemental weight % and atomic % of MAX phase Ti<sub>2</sub>AlC and Ti<sub>2</sub>CT<sub>x</sub> MXene. \* indicates the reduction of significant Al atomic percentage.

[9].

HRTEM was used to analyze the 2D crystal structure of Ti<sub>2</sub>CT<sub>x</sub> MXene. The bright field (BF) image taken at a low magnification allows the observation of the edges of a single Ti<sub>2</sub>CT<sub>x</sub> MXene flake (Fig. 2a) and the multilayered structure of differently oriented edges (Fig. 2b). The image of the layered reflection was also observable in the fast Fourier Transform (FFT) analysis taken from the edge-oriented particles (Fig. 2c). The inverse fast Fourier Transform (IFFT) show light and dark bands that alternate each other (Fig. 2 d). The bright bands indicate the layers of Ti–C–Ti for the case of Ti<sub>2</sub>C and the dark bands is related to the empty spacing between monolayers of the MXene flake that is formed after the removal of aluminum from the MAXphase.

### 3.2. X-ray diffraction spectra of Ti<sub>2</sub>AlC MAX phase and Ti<sub>2</sub>CT<sub>x</sub> MXene

The Ti<sub>2</sub>AlC MAX phase and Ti<sub>2</sub>CT<sub>x</sub> MXene was also characterised using XRD (Fig. 3). The diffraction peaks of Ti<sub>2</sub>AlC were identified at 10.8°, 12.8°, 15.7°, 17.8°, 19.4°, 20.2°, 23.7°, 26.2°, 33.6°, 39.3°, 41.7°, 43.2°, 52.9°, 56.3°, 60.4°, 65.3°, 71.6° and 74.6°. The diffraction peaks of Ti<sub>2</sub>CT<sub>x</sub> were identified at 5.1°, 10.8°, 13.0°, 15.9°, 17.1°, 18.8°, 22.1°, 25.0°, 31.9°, 35.9°, 37.9°, 41.6°, 47.7°, 56.3°, 60.5°, 72.4° and 76.8°. In comparison, no peak was identified at 39.3° for the XRD spectra of

Ti<sub>2</sub>CT<sub>x</sub> MXene, due to the removal of Al elements. The diffraction peaks were identified at 10.8°, 13.0°, 15.9°, 17.1°, 41.6°, 56.3°, and 60.5° of the Ti<sub>2</sub>CT<sub>x</sub> MXene were almost same peaks as found in the Ti<sub>2</sub>AlC MAX phase. This is due to unetched Ti<sub>2</sub>AlC MAX phase or small amount of Al apparent in the EDX analysis was present in Ti<sub>2</sub>CT<sub>x</sub> MXene. The Ti<sub>2</sub>CT<sub>x</sub> MXene nanosheets showed the basal plane peak had shifted to a lower 2θ angle, from 12.8° (d-spacing of 0.6902 nm) in the Ti<sub>2</sub>AlC precursor to 5.1° (d-spacing of 1.7145 nm). The lower peak shift of the basal planes occurs because of the removal of Al in the Ti<sub>2</sub>AlC and the presence of –F and –OH functional groups. Furthermore, the peak shift towards a lower angle of 5.1° suggested an increase in the interlayer d-spacing distance after ethanol treatment and ultra-sonication. These results agrees with a previous work reported by Ref. [9], confirming the successful synthesis of Ti<sub>2</sub>CT<sub>x</sub> MXene.

### 3.3. Chemical compositions of Ti<sub>2</sub>AlC MAX phase and Ti<sub>2</sub>CT<sub>x</sub> MXene

Fig. 4 presents the Raman spectra of Ti<sub>2</sub>AlC and pristine Ti<sub>2</sub>CT<sub>x</sub> MXene. The major Raman peaks of Ti<sub>2</sub>AlC MAX phase were determined at 98, 264 and 422 cm<sup>-1</sup>. These are assigned to the vibration modes of Ti and Al. The peak at 634 cm<sup>-1</sup> is attributed to the energy-gap modes of the in-plane Ti, C, as well as surface terminating functional groups. The

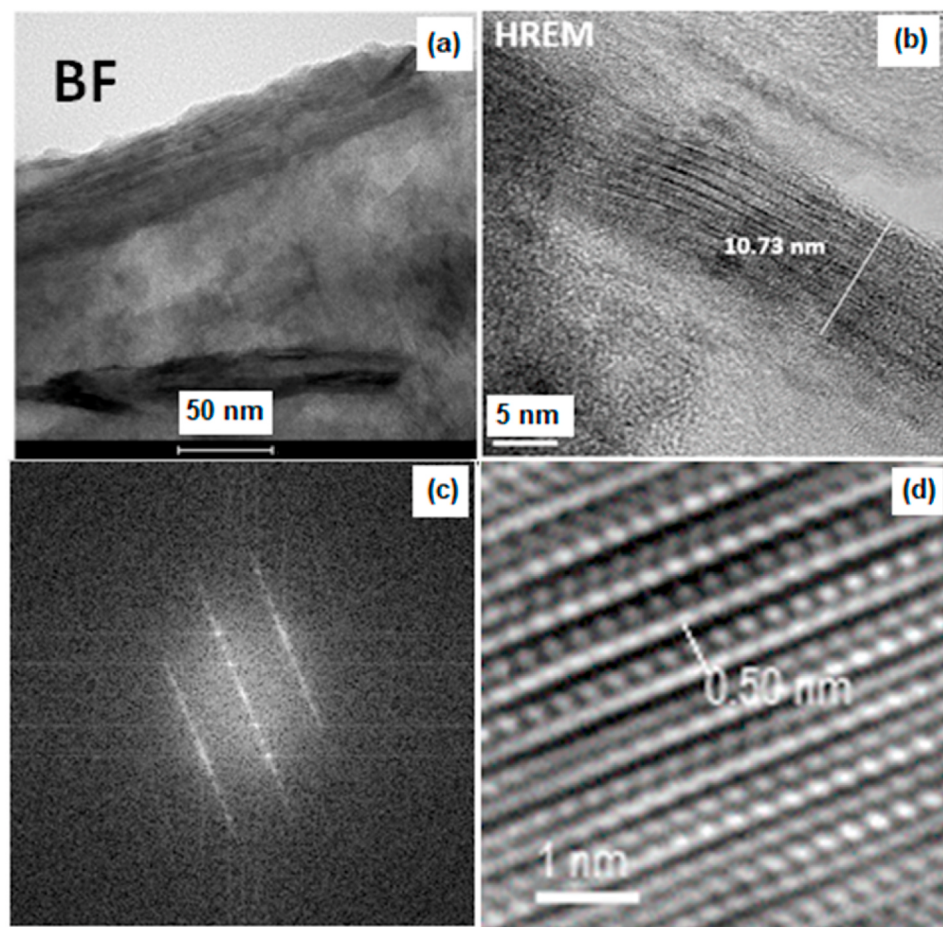


**Fig. 2.** (a) TEM image of a single 2D  $\text{Ti}_2\text{C}$  particles. HRTEM image of (b) flake edge and (c) the fast Fourier Transform (FFT), and (d) the inverse fast Fourier Transform (FFT) images.

Raman peaks of  $\text{Ti}_2\text{AlC}$  MAX phase at  $1326 \text{ cm}^{-1}$  and  $1574 \text{ cm}^{-1}$  were correlated to the D and G bands, which is indicative of the presence of free C [10]. The D band is related to the degree of disorder in graphite containing samples and a broad peak here suggests a slight disorder in the carbon of the material. In the  $\text{Ti}_2\text{CT}_x$  MXene, the peaks at  $279 \text{ cm}^{-1}$  and  $615 \text{ cm}^{-1}$  were associated with the energy-gap modes of the in-plane Ti, C and surface terminating functional groups. The peak at  $420 \text{ cm}^{-1}$  was attributed to the energy-gap modes of the in-plane Ti-O and Ti-OH surface terminating functional groups. The broadness peak at  $1563 \text{ cm}^{-1}$  indicates a slight disorder in the carbon of the MXene. Shifting of the characteristic peaks from  $\text{Ti}_2\text{AlC}$  MAX phase in  $\text{Ti}_2\text{CT}_x$  MXene were observed. The observed changes were correlated with XRD results, indicating that Al has been expunged from the  $\text{Ti}_2\text{AlC}$  MAX phase and replaced with other atoms. The  $\text{Ti}_2\text{CT}_x$  MXene produced consisting functional groups such as Ti-O, Ti-C, and Ti-OH allowed for unique interactions with the HeLa cell surface. It is known from previous studies that the Ti-O, Ti-C, and Ti-OH functional groups increase the adsorption of proteins and other biomolecules on the cell membrane of HeLa [11,12]. Therefore, the physical interactions between MXene and HeLa cells is of special interest and this is further investigated.

### 3.4. Zeta potential and DLS measurement

The pristine 2D  $\text{Ti}_2\text{C}$  MXene phase defragmented by sonication into the multilayered structure had the lowest zeta potential value  $-10 \text{ mV}$  (Fig. 5 (a), 1:0 wt ratio, marked with yellow colour). This indicates that the sonication process failed to yield a fully stable colloid of multilayered 2D particles in an aqueous solution. The same problem was

described for multilayer structures of both  $\text{Ti}_2\text{C}$  and  $\text{Ti}_3\text{C}_2$  [5,6]. 2D  $\text{Ti}_2\text{C}$  phase modified with  $\text{CaCl}_2$  in the 1:1 wt ratio, yield better stability of about  $-17 \text{ mV}$ . However, when compared to chemically delaminated single- or few-layered  $\text{Ti}_3\text{C}_2\text{T}_x$  particles with recorded stabilities of about  $-45$  or  $-50 \text{ mV}$ , the steady state is difficult to achieve [12–14]. Therefore, it is essential to test the stability of 2D  $\text{Ti}_2\text{C}$  particles after interaction with the alginate as alginate was applied during the process of microencapsulation of 3D cells. Strikingly, we have observed that even a small addition of sodium alginate caused a significant increase of MXene stability up to the value of about  $-43 \text{ mV}$ . This proved that the systems based on sodium alginate in small amounts stabilizes the MXene and also, surface-stabilized MXene would strongly interact with structures having positive surface charges. In addition, the further addition of the sodium alginate to 2D  $\text{Ti}_2\text{C}$  MXene caused another significant increase of stability up to the value of about  $-61 \text{ mV}$  (this refers to 1:20 wt ratio). This enables the MXene/alginate system highly promising for supporting biological interactions. To the best of our knowledge, this is the lowest zeta potential value ever reported for MXenes.

To further confirm the stability of 2D  $\text{Ti}_2\text{C}$  MXene, we further investigated the hydrodynamic diameter of MXene treated with alginate using the DLS technique. From the obtained distributions of diameters, we have extracted the mean values for nano-fraction of 2D particles. These presence of the nano-fraction of particles was already confirmed with HREM studies (see Fig. 2b). Such particles, if non-stable, readily agglomerate causing gradual sedimentation which is non favourable for biomedical application. This barely noticeable effect can be easily identified and observed *in situ* with a very sensitive DLS technique. The micro-fraction of 2D particles rapidly sediments which makes

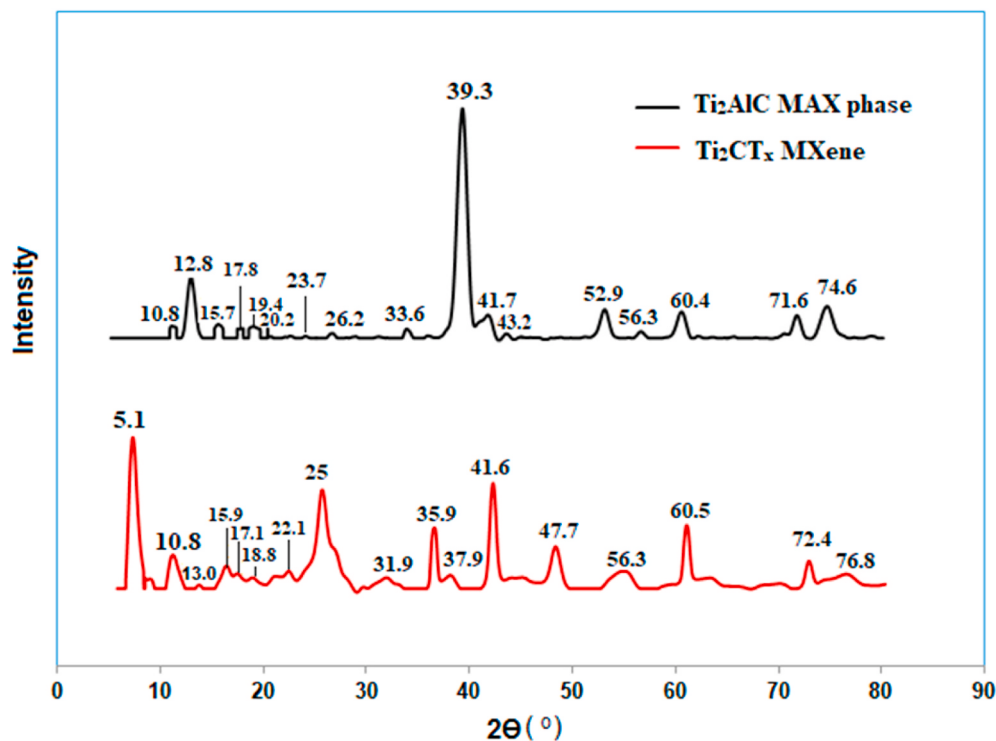


**Fig. 3.** XRD patterns of Ti<sub>2</sub>AlC MAX phase (black line) and Ti<sub>2</sub>CT<sub>x</sub> MXene (red line). (For interpretation of the references to colour in this figure legend, the reader is referred to the Web version of this article.)

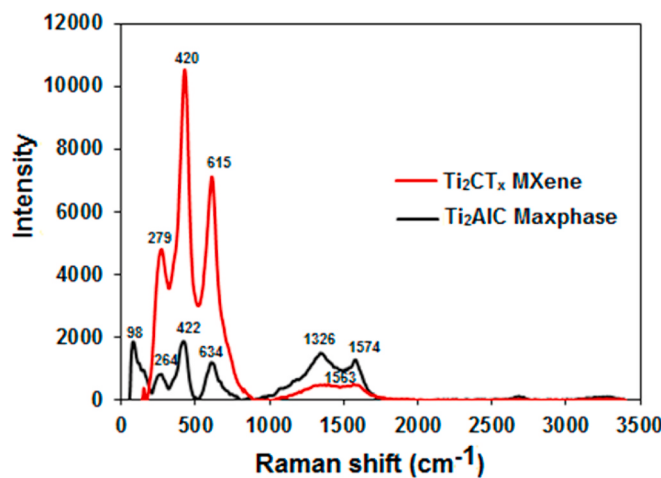


**Fig. 4.** Raman spectra of Ti<sub>2</sub>AlC MAX phase and Ti<sub>2</sub>CT<sub>x</sub> MXene

difficulties for *in situ* observations. Non-modified 2D Ti<sub>2</sub>C particles (1:0 wt ratio, marked with yellow colour) had an average hydrodynamic diameter of about 200 nm (Fig. 5b). Modification with CaCl<sub>2</sub> (1:1 wt ratio, marked with red colour) caused its decrease to about 100 nm (Fig. 5b). While introducing the sodium alginate to the MXene colloid, the hydrodynamic diameter dropped to about 70 nm with a slight increase at 1:4 wt ratio. This effect is a clear reflection of deagglomeration of 2D particles nano-fraction. Then, in the case of a very high alginate addition (1:20 wt ratio), the hydrodynamic rapidly went back to about 200 nm. This indicates the development of a large alginate layer of the surface of 2D Ti<sub>2</sub>C particles which adhered particles to each other.

### 3.5. FTIR results

The formation of the alginate layer on the surface of 2D Ti<sub>2</sub>C particles

was further confirmed by FTIR spectroscopy (Fig. 5c). The non-modified 2D Ti<sub>2</sub>C particles expressed a wide band at about 3500 cm<sup>-1</sup>, associated with the presence of characteristic –OH functional groups. Also, a peak at 562 cm<sup>-1</sup> was identified, indicate surface Ti–O bonds [15]. In a case of 2D Ti<sub>2</sub>C/sodium alginate (weight ratio of 1:1), a peak at 316 cm<sup>-1</sup> derived from the alginate –OH groups was observed together with a peak at 2359 cm<sup>-1</sup>, associated with the presence of O=C=O stretching vibrations. Other alginate-related peaks constitute 1603 cm<sup>-1</sup> and 1417 cm<sup>-1</sup> associated with the -COO<sup>-</sup> asymmetric and symmetric vibrations, respectively. The peak at 1095 cm<sup>-1</sup> was further associated with the occurrence of alginate C=O bonds [16]. The addition of CaCl<sub>2</sub> to the system in a weight ratio of 1:1:0.5, resulted in the formation of 2D Ti<sub>2</sub>C/calcium alginate. In this study, apart from chemical species described above, we observed only much higher signal form –OH groups because of strong hygroscopic properties of CaCl<sub>2</sub>. There were no other interactions between tested components.

### 3.6. UV–Vis

The complimentary UV–Vis spectra were recorded for pristine 2D Ti<sub>2</sub>C MXene as well as 2D Ti<sub>2</sub>C/sodium alginate (1:1 wt ratio) and 2D Ti<sub>2</sub>C/calcium alginate (1:1:0.5 wt ratio). The non-modified MXene showed the highest transmittance of about 89% at a 420–620 nm wavelength (Fig. 5d). The 2D Ti<sub>2</sub>C/sodium alginate had a transmittance of 87% at the same wavelength as the pure MXene. This indicated a slight weakening of light transmission by the surface-modified sample, but with no adsorption shift. In a case of 2D Ti<sub>2</sub>C/calcium alginate, numerous peak variations are present in the spectrum, confirming the structural changes in when adding sodium alginate [17].

### 3.7. Cellular interactions of Ti<sub>2</sub>CT<sub>x</sub> MXenes

The cellular interactions of the pristine 2D Ti<sub>2</sub>CT<sub>x</sub> MXenes were observed after 24 h of incubation with materials at either 50 µg/mL or 500 µg/mL by using inverted phase contrast microscopic (Fig. 6). The

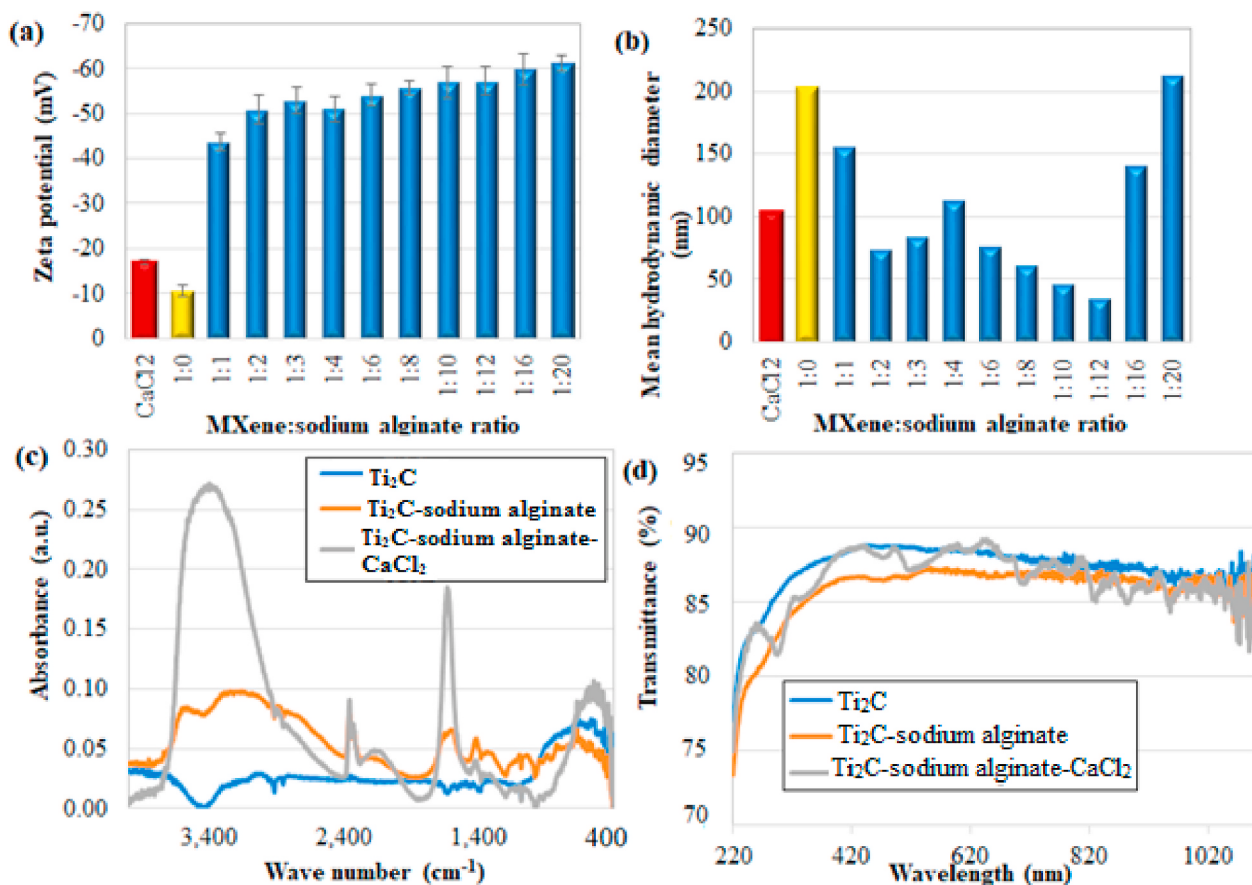


**Fig. 5.** Colloidal stability characterization of 2D  $\text{Ti}_2\text{C}$  particles in the presence of sodium alginate and  $\text{CaCl}_2$  for distilled water-based dispersions, involving (a) zeta potential,(b) DLS studies. Physicochemical characterization of 2D  $\text{Ti}_2\text{C}$  particles in the presence of sodium alginate and  $\text{CaCl}_2$  for distilled water-based dispersions, analyzed by (c) FTIR and (d) UV-Vis.

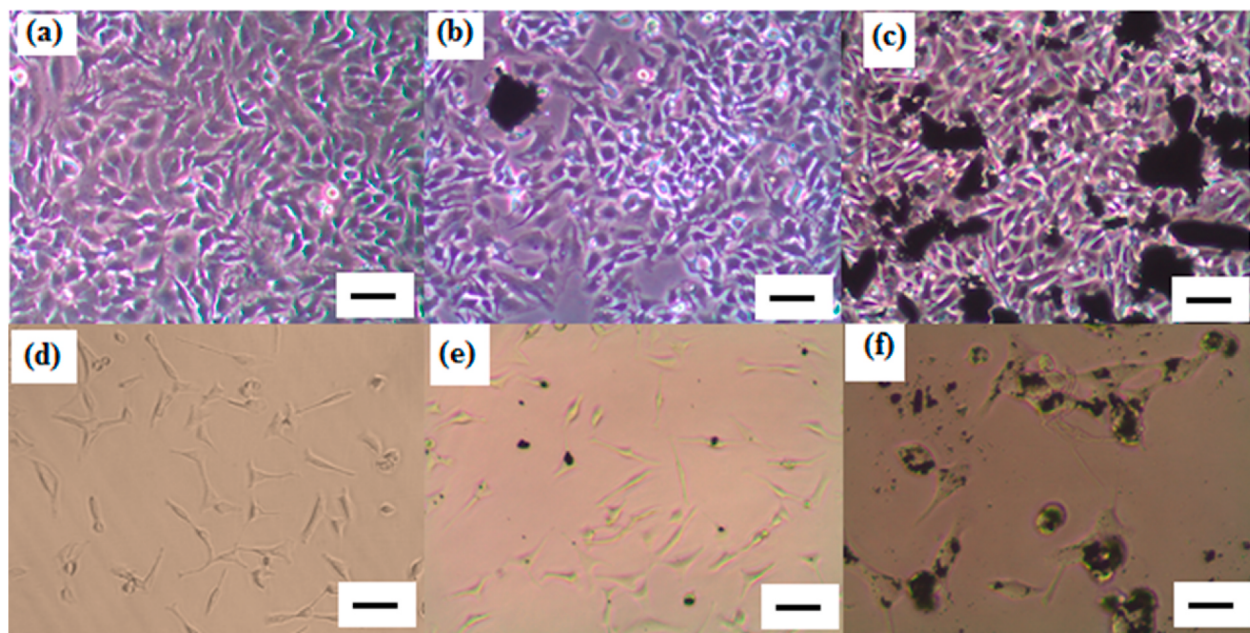


**Fig. 6.** Phase contrast images of confluent HeLa cells with (a) control, (b) 50  $\mu\text{g}/\text{mL}$ , and (c) 500  $\mu\text{g}/\text{mL}$  of the MXenes. Bright field images of low density of HeLa cells treated with (d) control, (e) 50  $\mu\text{g}/\text{mL}$ , and (f) 500  $\mu\text{g}/\text{mL}$  of the  $\text{Ti}_2\text{CT}_x$  MXenes. (scale bar: 50  $\mu\text{m}$ )

micrographs also allow inspection of the morphological change and any cellular membrane damage that could have been induced by the MXenes. In the microscopic images, HeLa cells show a normal and spindle like morphology in the control and treatment at 50 µg/mL of Ti<sub>2</sub>CT<sub>x</sub> MXenes (Fig. 6a and b). When the HeLa cells were exposed to a higher concentration of Ti<sub>2</sub>CT<sub>x</sub> MXenes, it can be observed that MXenes possess the strong binding capacity to the cellular membranes of HeLa cells (Fig. 6c). This is probably due to interaction of the negative zeta potential of the MXenes with positively charged proteins found on the surface of the cell membrane. In the bright field images of the control and 50 µg/mL Ti<sub>2</sub>CT<sub>x</sub> MXenes, no significant morphological change of cells were observed due to the amount of MXenes applied could be neglected (Fig. 6d and e). However, significant agglomeration of Ti<sub>2</sub>CT<sub>x</sub> MXenes at higher concentrations (500 µg/mL) on rounded HeLa cells was observed (Fig. 6f). Similar results were reported when Ti<sub>2</sub>C-PEG MXene were applied to cancerous cells [5]. Nevertheless, further study is needed to confirm the cytotoxicity of MXene in normal cells.

### 3.8. Cytotoxicity activity of MXenes to 2D and 3D HeLa cells

The cytotoxicity activity of the Ti<sub>2</sub>CT<sub>x</sub> MXenes was determined using a cervical cancer cell line (HeLa) in 2D and 3D cells model system. After 24 h of exposure, the cell viability of HeLa cells, exposed to Ti<sub>2</sub>CT<sub>x</sub> MXenes, decreased from 98% to 43% with an increasing Ti<sub>2</sub>CT<sub>x</sub> MXenes concentration from 50 to 300 µg/mL (Fig. 7a). Further increases of the Ti<sub>2</sub>CT<sub>x</sub> MXenes concentrations from 300 to 500 µg/mL show no noticeable difference of cell viability. From the results, we observed that cytotoxicity of Ti<sub>2</sub>CT<sub>x</sub> MXenes to HeLa cells was dose-dependent. For further confirmation of the dose-dependent cytotoxicity of Ti<sub>2</sub>CT<sub>x</sub> MXenes to HeLa cells, cell viability was characterized using Muse® Count & Viability reagent. Fig. 7b shows the cells viability after 24 h treatment with different concentrations of the Ti<sub>2</sub>CT<sub>x</sub> MXenes (50–500 µg/mL) on HeLa cells. The cell viability decreased almost to a half with an increased concentration of the Ti<sub>2</sub>CT<sub>x</sub> MXenes (from 91% to 53% in 500 µg/mL of MXene treatment). The decline in cell viability was suggested due to the direct physicochemical interactions of Ti<sub>2</sub>CT<sub>x</sub> MXenes

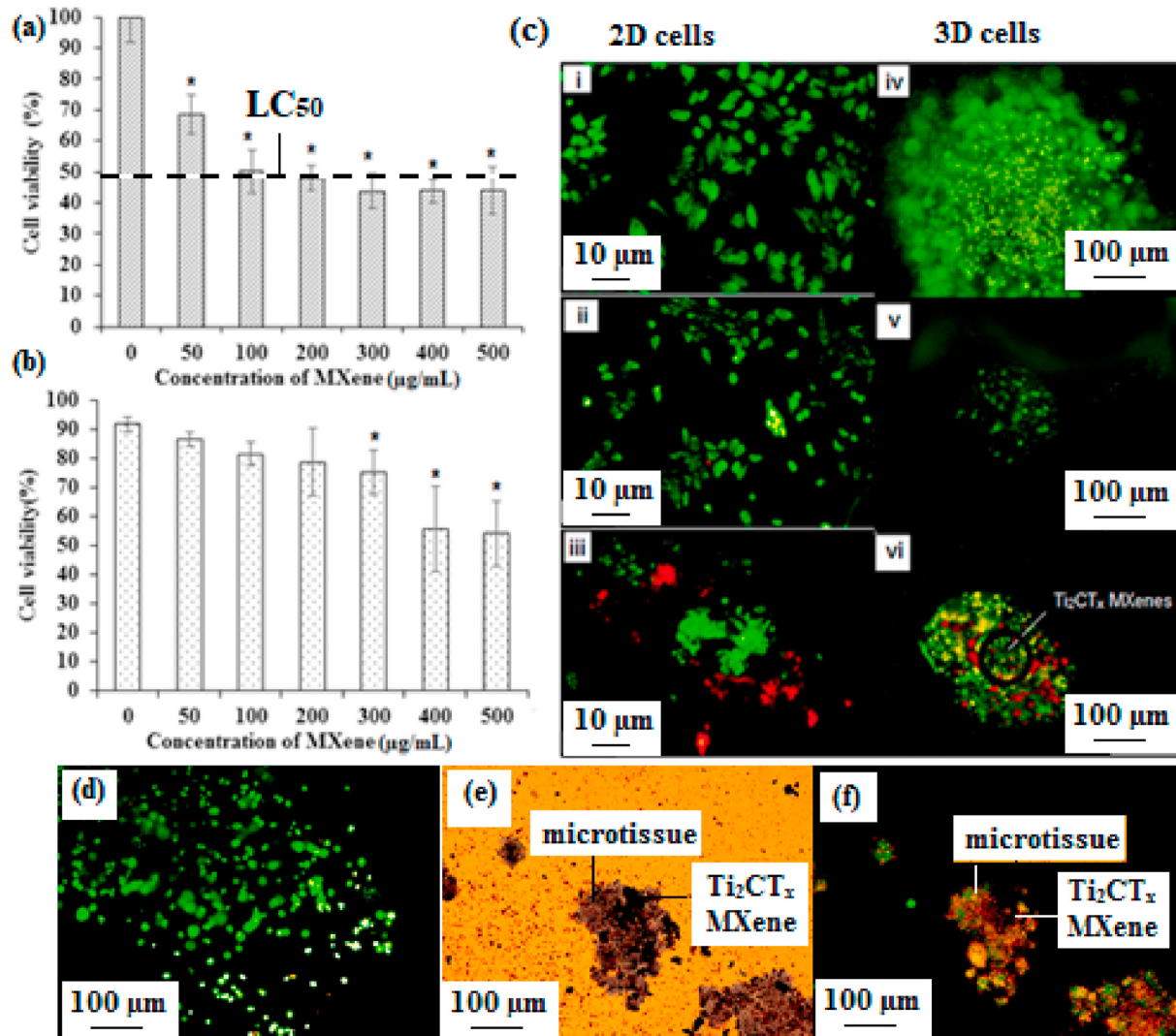


**Fig. 7.** The results of cytotoxicity studies: cells viability after 24 h treatment with different concentrations of the Ti<sub>2</sub>CT<sub>x</sub> MXenes (50–500 µg/mL) on HeLa cells, measured using (a) MTT assay and (b) Muse® Cell flow cell cytometer. The results presented are the mean of three independent experiments and the error bars shown represent the standard deviation with  $n = 3$ . It is also \* $p < 0.05$  indicates significant to control, using Student independent  $t$ -test. (c) Live and dead cell staining images of 2D HeLa cells after 24 h exposure with (i) control, (ii) 50 µg/mL, and (iii) 500 µg/mL of the Ti<sub>2</sub>CT<sub>x</sub> MXenes. Fluorescence images of 3D HeLa cells encapsulated in alginate microbeads with (iv) control, (v) 50 µg/mL, and (vi) 500 µg/mL of the Ti<sub>2</sub>CT<sub>x</sub> MXenes. The living and dead cells are respectively marked by green and red fluorescent colors. Image (e) in a bright field of 3D micro tissues with 500 µg/mL of the Ti<sub>2</sub>CT<sub>x</sub> MXenes. The magnification of all images is 20×. (For interpretation of the references to colour in this figure legend, the reader is referred to the Web version of this article.)

with the cell membranes, inhibiting the HeLa cells proliferation (Fig. 6c and f). The results of MTT assay and Muse flow cytometer strongly aligned, indicating only half of cell viability observed in 500 µg/mL MXene treatment (Fig. 5a and b). This is proven that the pristine 2D Ti<sub>2</sub>CT<sub>x</sub> MXene is moderately cytotoxic to HeLa cells and the level of cytotoxicity is dose-dependent. These results are in agreement with the previous report where cancerous cells (A549 and A375) decreased with an increasing concentration of DMSO delaminated Ti<sub>3</sub>C<sub>2</sub>T<sub>x</sub> [3]. Live and dead cell staining results show high viability of HeLa cells grown in cultured medium without Ti<sub>2</sub>CT<sub>x</sub> MXenes and 50 µg/mL Ti<sub>2</sub>CT<sub>x</sub> MXenes treatment (Fig. 7C). Further increase in the concentration of Ti<sub>2</sub>CT<sub>x</sub> MXene to 500 µg/mL resulted in almost 50% cell death. The live/dead cells staining results agreed with initial cytotoxicity assay results and suggests the only low cytotoxicity of a low concentration of MXenes, and cytotoxicity only becomes apparent at treatment with 500 µg/mL of Ti<sub>2</sub>CT<sub>x</sub> MXene.

We further evaluated the cytotoxicity of Ti<sub>2</sub>CT<sub>x</sub> MXene in 3D cell cultures by dispersing the 50 µg/mL and 500 µg/mL of the Ti<sub>2</sub>CT<sub>x</sub> MXene to the Hela cells encapsulated in alginate microbeads. Fig. 5c (iv) indicates that the cells grown into microtissues were still highly viable after 15 days of culture in control and also 50 µg/mL Ti<sub>2</sub>CT<sub>x</sub> MXenes treatment. However, some cells were found non-viable when 3D cells were incubated with 500 µg/mL of the Ti<sub>2</sub>CT<sub>x</sub> MXenes (Fig. 5c (vi)). On the other hand, some dead cells were observed in the specific area of alginate microcapsule where the agglomerates of attached Ti<sub>2</sub>CT<sub>x</sub> MXenes (Fig. 5c (vi)). The stable adhesion of the MXene on the alginate surface depriving the exposure of gases and ions at a localized area of the alginate surface where the MXene was attached. Our zeta potential results have predicted the adhesiveness of the 2D MXene to alginate, as observed in this part of the investigation. In order to evaluate the direct physicochemical interactions of Ti<sub>2</sub>CT<sub>x</sub> MXene with the cell membrane as the mechanisms of Ti<sub>2</sub>CT<sub>x</sub> MXenes toxicity, the alginate shell of the alginate microbeads of HeLa cells was removed by using alginate lyase, and the 3D microtissues released from the alginate shell were treated with 500 µg/mL of the Ti<sub>2</sub>CT<sub>x</sub> MXenes. The microtissues were highly viable after 15 days of culture when released from alginate shell using alginate lyase (Fig. 7d). The results of live and dead staining showed that the dead cells were observed in the area where the agglomerates of Ti<sub>2</sub>CT<sub>x</sub> MXenes directly bound to the surface of the 3D micro tissues (Fig. 7 (e) and (f)). The direct adhesion of Ti<sub>2</sub>CT<sub>x</sub> MXenes to the cell membrane of microtissues, limit the growth of microtissues and cell division, resulting in lower cell viability.

### 3.8.1. Oxidative stress assays

Fig. 8(a) and (b) present the ROS negative (−) and positive (+) generations at different concentrations (50–500 µg/mL) of Ti<sub>2</sub>CT<sub>x</sub>

MXenes. Fig. 8 clearly indicates no changes of ROS level between control and Ti<sub>2</sub>CT<sub>x</sub> MXenes treated cells at all concentrations. The results suggest that the MXene did not induce oxidative stress to the cells. In considering previous cytotoxicity assays results (Fig. 7), this study suggests that the cytotoxicity pathways of Ti<sub>2</sub>CT<sub>x</sub> MXene was strongly not associated with the oxidative stress but was influenced by the direct physicochemical interactions of Ti<sub>2</sub>CT<sub>x</sub> MXene with the cell membrane (Fig. 6). From our previous findings, where a significant increase in ROS level was observed in Ti<sub>2</sub>C/PEG treated cancer cell lines (A549 and 375) [5]. This is because direct physicochemical interactions tend to induce oxidative stress in cells, which leads to cell damage and death. By comparing our findings with previous studies [3,5], cellular response after exposure to MXene treatments were indeed different due to the many inherent different characteristics between cancer cells, which is typically due to their different cell metabolism. The cellular responses of cells can be different after exposure to different structures of MXenes.

In the further investigation of the physical interactions of Ti<sub>2</sub>CT<sub>x</sub> MXenes and HeLa cells, FE-SEM images revealed a strong adhesion of MXenes to the monolayer membrane of HeLa cells (Fig. 9). This may be due to the surface charges or functional groups present on the surface of the MXenes that promote molecular binding to the cell-surface integrin receptors. The untreated HeLa cells show a broadly spread and spindle-like structure (Fig. 9b). In Fig. 9(c) and (d), multilayered MXene seem to settle on the surface of cells. A similar effect was observed for Ti<sub>3</sub>C<sub>2</sub>T<sub>x</sub> MXenes, due to the strong binding of the MXenes to HeLa cellular membranes, the SEM images demonstrated that the cells cannot absorb the large MXene structures, lastly causing damage to the membrane and also cytoskeletal structure [4]. In this study, the attachment of Ti<sub>2</sub>CT<sub>x</sub> on the cells influences the morphology and inhibits the spread of the HeLa cells. This could be due to the binding of the MXene to the cell surface integrin receptors that has disrupted the cell mechanotransduction, thus, leading to the failure in lamellipodia extension (Figs. 6f and 9c). The pristine 2D Ti<sub>2</sub>CT<sub>x</sub> MXenes were indicated with a negative zeta potential value of −10 mV. The cell-surface integrin receptors are made from transmembrane proteins that could present a high affinity to the MXene particles. The Ti<sub>2</sub>CT<sub>x</sub> MXenes with a negative charge resulting from Ti-OH, Ti-O, and Ti-F surface functional groups can interact with cell-surface integrin receptors positively that has inhibited the functionality of focal adhesions and hence, reduced the protrusion of cell membrane.

The Raman spectra of HeLa cells consists of two regions; the finger-print region which span 400–1800 cm<sup>−1</sup> and the high wavenumber region which span 2500–3500 cm<sup>−1</sup>. This is apparent in Fig. 10. The peak observed at 548 cm<sup>−1</sup> was due to the presence of cholesterol (Fig. 10 a). The spectra peak at 678 cm<sup>−1</sup> is possibly associated with the ring breathing mode in the deoxyribonucleic acid (DNA) bases [18]. The

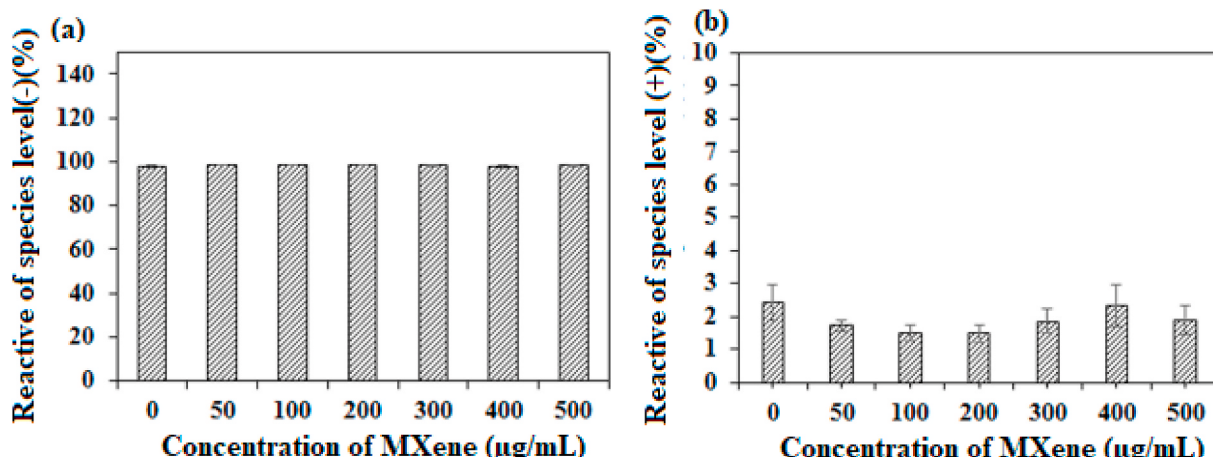


Fig. 8. The intracellular ROS levels (−) and (+) after 24 h of exposure to different concentrations of the Ti<sub>2</sub>CT<sub>x</sub> MXenes on HeLa cells in 2D cell culture.

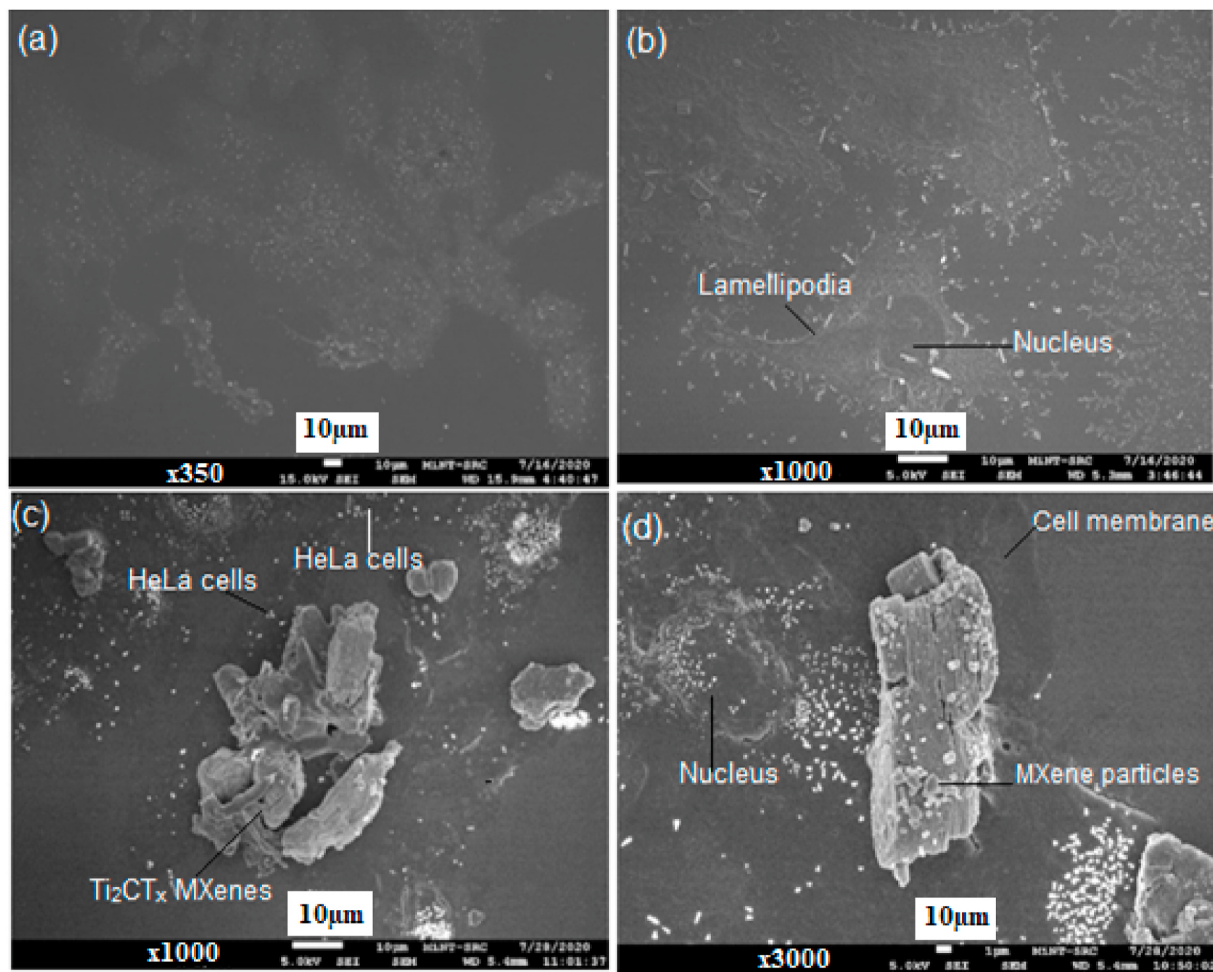


Fig. 9. FE-SEM micrographs of HeLa cells in (a–b) control and (c–d) in 2D cell culture after exposure to 500 µg/mL of  $\text{Ti}_2\text{CT}_x$  MXenes, respectively.

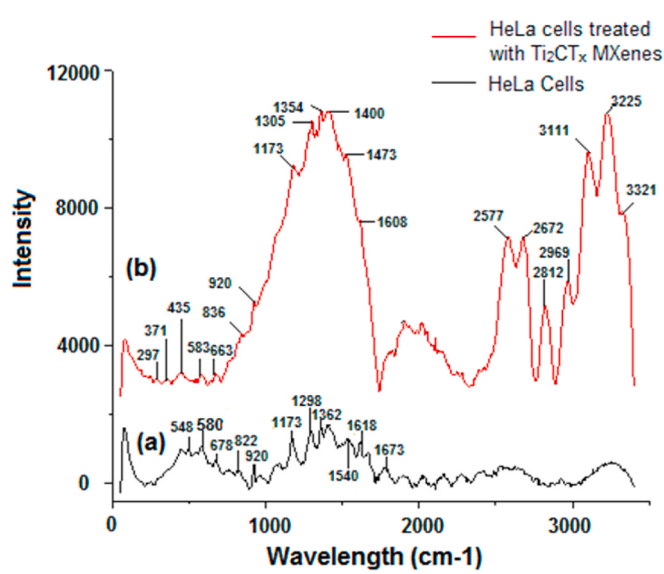


Fig. 10. Raman spectra of (a) control treated HeLa cells and (b) 500 µg/mL of  $\text{Ti}_2\text{CT}_x$  MXenes treated HeLa cells in 2D cell culture.

peak positioned at  $822 \text{ cm}^{-1}$  was attributed to the Phosphodiester of DNA. The Raman peak identified at  $920 \text{ cm}^{-1}$  was attributed to the C–C stretching of the proline ring in collagen. The peak of  $1173 \text{ cm}^{-1}$  was

assigned to cytosine and guanine tyrosine of Collagen type I. The peak at  $1298 \text{ cm}^{-1}$  was attributed to the acyl chains as well as the fatty and palmitic acid. The Raman spectra at  $1362 \text{ cm}^{-1}$  were assigned to Guanine. The Raman peaks observed at  $1540 \text{ cm}^{-1}$  and  $1673 \text{ cm}^{-1}$  respectively indicate vibration due to the amide carbonyl group [19]. The peak at  $1618 \text{ cm}^{-1}$  was attributed to tryptophan. Fig. 10b shows the Raman spectra for HeLa cells that have been treated with  $\text{Ti}_2\text{CT}_x$  MXenes. There was a large broad peak observed in between  $900$  and  $1700 \text{ cm}^{-1}$  for HeLa cells treated with MXene, suggesting that the  $\text{Ti}_2\text{CT}_x$  MXenes had adsorbed to the HeLa cells surface. In the  $\text{Ti}_2\text{CT}_x$  MXene, the peaks assigned at  $279 \text{ cm}^{-1}$ ,  $420 \text{ cm}^{-1}$  and  $615 \text{ cm}^{-1}$  were assigned to the energy-gap modes of the in-plane Ti, C, Ti-OH, and Ti-O surface functional groups (Fig. 4). It was noticed that the shifting of the characteristic peaks from  $\text{Ti}_2\text{CT}_x$  MXene in HeLa cells treated with  $\text{Ti}_2\text{CT}_x$  MXene. The change in the Raman shift of these peaks, we inferred that  $\text{Ti}_2\text{CT}_x$  MXenes had adsorbed to the HeLa cells surface. The Raman peaks HeLa cells treated with  $\text{Ti}_2\text{CT}_x$  MXene observed at  $583 \text{ cm}^{-1}$ ,  $663 \text{ cm}^{-1}$ , and  $836 \text{ cm}^{-1}$  were assigned to the Phosphodiester of DNA and cholesterol. This observation may imply that the structure of the DNA double helix and cell membrane changed after the exposure to  $\text{Ti}_2\text{CT}_x$  MXenes [20]. The Raman band observed at  $1173 \text{ cm}^{-1}$  associated with the collagen type-I did not change the peak position, but the intensity increased after the  $\text{Ti}_2\text{CT}_x$  MXenes treatment. The Raman peaks that were previously observed at  $1540 \text{ cm}^{-1}$  and  $1670 \text{ cm}^{-1}$  is not here, which suggests that the protein and nucleic acid may have been destroyed due to exposure to a high concentration of the  $\text{Ti}_2\text{CT}_x$  MXene. The Raman peaks found in the range of  $2500$ – $3500 \text{ cm}^{-1}$   $\text{Ti}_2\text{CT}_x$  MXenes were related to the C–H, N–H, and O–H stretching vibrations in the protein and lipid structures

[19,21]. The Raman spectroscopy indicated that the  $Ti_2CT_x$  MXenes may disrupt the conformation of the proteins in the cytoplasm and blocking the cell surface proteins, causing changes in the biochemical processes, mechano-transduction, cell membrane disruption, as well as apoptosis [20].

#### 4. Conclusion

MXenes are a class of emerging 2-D material that show great promise in biomedical applications due to their unique beneficial characteristics. However, there still exist a lack of study on the possible toxicity effects of MXenes on cells; therefore, the present study was carried out to address this issue. This study reveals important findings regarding the *in vitro* cytotoxicity of  $Ti_2CT_x$  MXenes against HeLa cells by using 2D and 3D model cells that better mimic real physiological conditions. When in contact with the HeLa cells,  $Ti_2CT_x$  MXene effectively inhibits the cellular function of HeLa cells and causes massive cellular changes as shown in the Raman spectra. This study is an advancement in the development of safe MXene-based technologies for biomedical applications.

#### Declaration of competing interest

The authors declare that they have no known competing financial interests or personal relationships that could have appeared to influence the work reported in this paper.

#### Acknowledgment

This project is funded by the Ministry of Higher Education Malaysia under the Research Excellence Consortium Grant Scheme (KKP) or KPM-special grant RMK-10 with a reference number of KKP Vot. No. K343. The HREM, UV-VIS, FTIR, and zeta potential studies were funded by The National Science Centre, grant ‘OPUS 18’ with a reference number of UMO-2019/35/B/ST5/02538. The authors also acknowledge the technical support from Faezahana Mohkter and Ahmad Nasrull Mohamed.

#### References

- [1] B. Anasori, M.R. Lukatskaya, Y. Gogotsi, 2D metal carbides and nitrides (MXenes) for energy storage, *Nature Reviews Materials* 2 (2) (2017) 1–17.
- [2] K. Rasool, M. Helal, A. Ali, C.E. Ren, Y. Gogotsi, K.A. Mahmoud, Antibacterial activity of  $Ti_3C_2T_x$  MXene, *ACS Nano* 10 (3) (2016) 3674–3684.
- [3] A.M. Jastrzębska, A. Szuplewska, T. Wojciechowski, M. Chudy, W. Ziemkowska, L. Chlubny, A. Olszyna, In vitro studies on cytotoxicity of delaminated  $Ti_3C_2$  MXene, *J. Hazard Mater.* 339 (2017) 1–8.
- [4] B. Scheibe, J.K. Wychowaniec, M. Scheibe, , Peplińska, B., M. Jarek, G. Nowaczyk, L. Przyświecka, Cytotoxicity assessment of Ti-Al-C based MAX phases and  $Ti_3C_2T_x$  MXenes on human fibroblasts and cervical cancer cells, *ACS Biomater. Sci. Eng.* 5 (12) (2019) 6557–6569.
- [5] A. Szuplewska, D. Kulpińska, A. Dybko, A.M. Jastrzębska, T. Wojciechowski, A. Rozmysłowska, A. Olszyna, 2D  $Ti_2C$  (MXene) as a novel highly efficient and selective agent for photothermal therapy, *Mater. Sci. Eng. C* 98 (2019) 874–886.
- [6] A. Rozmysłowska-Wojciechowska, T. Wojciechowski, W. Ziemkowska, L. Chlubny, A. Olszyna, A.M. Jastrzębska, Surface interactions between 2D  $Ti_3C_2/Ti_2C$  MXenes and lysozyme, *Appl. Surf. Sci.* 473 (2019) 409–418.
- [7] A. Rozmysłowska-Wojciechowska, J. Mitrak, A. Szuplewska, M. Chudy, J. Woźniak, M. Petrus, A.M. Jastrzębska, Engineering of 2D  $Ti_3C_2$  MXene surface charge and its influence on biological properties, *Materials* 13 (10) (2020) 2347.
- [8] A. Rozmysłowska-Wojciechowska, A. Szuplewska, T. Wojciechowski, S. Pońskiak, J. Mitrak, M. Chudy, A.M. Jastrzębska, A simple, low-cost and green method for controlling the cytotoxicity of MXenes, *Mater. Sci. Eng. C* 110790 (2020).
- [9] K. Zhu, Y. Jin, F. Du, S. Gao, Z. Gao, X. Meng, Y. Gao, Synthesis of  $Ti_2CT_x$  MXene as electrode materials for symmetric supercapacitor with capable volumetric capacitance, *Journal of energy chemistry* 31 (2019) 11–18.
- [10] I. Habib, P. Ferrer, S.C. Ray, K.I. Ozoemena, Interrogating the impact of onion-like carbons on the supercapacitive properties of MXene ( $Ti_2CT_x$ ), *J. Appl. Phys.* 126 (13) (2019) 134–301.
- [11] M. Xu, J. Zhu, F. Wang, Y. Xiong, Y. Wu, Q. Wang, J. Weng, Z. Zhang, W. Chen, S. J. Liu, Improved *in vitro* and *in vivo* biocompatibility of graphene oxide through surface modification: poly(acrylic acid)-functionalization is superior to PEGylation, *ACS Nano* 10 (3) (2016) 3267–3281.
- [12] M. Zhou, N. Lozano, J.K. Wychowaniec, T. Hodgkinson, S.M. Richardson, K. Kostarelos, J.A. Hoyland, Graphene oxide: a growth factor delivery carrier to enhance chondrogenic differentiation of human mesenchymal stem cells in 3D hydrogels, *Acta Biomater.* 96 (2019) 271.
- [13] X. Zhao, A. Vashisth, E. Prehn, W. Sun, S.A. Shah, T. Habib, M.J. Green, Antioxidants unlock shelf-stable  $Ti_3C_2T_x$  (MXene) nanosheet dispersions, *Matter* 1 (2) (2019) 513–526.
- [14] Z. Zeng, C. Wang, G. Siqueira, D. Han, A. Huch, S. Abdolhosseinzadeh, J. Heier, F. Nüesch, C.(J.) Zhang, G. Nyström, Nanocellulose-MXene biomimetic aerogels with orientation-tunable electromagnetic interference shielding performance, *Adv. Sci.* 7 (15) (2020) 2000979.
- [15] W. Zhi, S. Xiang, R. Bian, R. Lin, K. Wu, T. Wang, D. Cai, Study of MXene-filled polyurethane nanocomposites prepared via an emulsion method, *Compos. Sci. Technol.* 168 (2018) 404–411.
- [16] S.K. Papageorgiou, E.P. Kouvelos, E.P. Favvas, A.A. Sapalidis, G.E. Romanos, F. K. Katsaros, Metal–carboxylate interactions in metal–alginate complexes studied with FTIR spectroscopy, *Carbohydr. Res.* 345 (4) (2010) 469–473.
- [17] Y. Huang, H. Yang, Y. Zhang, Y. Zhang, Y. Wu, M. Tian, Y. Wu, A safe and fast-charging lithium-ion battery anode using MXene supported  $Li_3VO_4$ , *J. Mater. Chem.* 7 (18) (2019) 11250–11256.
- [18] C.H. Liu, B. Wu, L.A. Sordillo, S. Boydston-White, V. Sriramouji, C. Zhang, R. R. Alfano, A pilot study for distinguishing basal cell carcinoma from normal human skin tissues using visible resonance Raman spectroscopy, *J. Cancer Metastasis Treat.* 5 (2019) 4.
- [19] F.M. Lyng, D. Traynor, I.R. Ramos, F. Bonnier, H.J. Byrne, Raman spectroscopy for screening and diagnosis of cervical cancer, *Anal. Bioanal. Chem.* 407 (27) (2015) 8279–8289.
- [20] N. Xu, P. Zhu, J. Liang, L. Liu, W. Zhang, X. Li, Y. He, Label-free Raman spectroscopy monitoring of cytotoxic response induced by a telomerase inhibitor, *Sensors and Actuators B: Chemicals* 293 (2019) 1–10.
- [21] Z. Movasagh, S. Rehman, I.U. Rehman, Raman spectroscopy of biological tissues, *Appl. Spectrosc. Rev.* 42 (5) (2007) 493–541.